View Article Online / Journal Homepage / Table of Contents for this issue



# SAXS investigation of a cubic to a sponge ($L_3$) phase transition in self-assembled lipid nanocarriers†

**Borislav Angelov,[ab] Angelina Angelova,*[c] Rada Mutafchieva,[d] Sylviane Lesieur,[c] Ulla Vainio,[e] Vasil M. Garamus,[f] Grethe V. Jensen[a] and Jan Skov Pedersen[a]**

***Received 30th June 2010, Accepted 19th October 2010***
**DOI: 10.1039/c0cp01029d**

Published on 16 November 2010. Downloaded by Lund University on 03/12/2014 13:54:28.

The encapsulation and release of peptides, proteins, nucleic acids, and drugs in nanostructured lipid carriers depend on the type of the self-assembled liquid-crystalline organization and the structural dimensions of the aqueous and membraneous compartments, which can be tuned by the multicomponent composition of the systems. In this work, small-angle X-ray scattering (SAXS) investigation is performed on the 'melting' transition of the bicontinuous double diamond cubic phase, formed by pure glycerol monooleate (MO), upon progressive inclusion of varying fractions of pharmaceutical-grade glycerol monooleate (GO) in the hydrated system. The self-assembled MO/GO mixtures are found to form diamond (*Pn*3*m*) inverted cubic, inverted hexagonal ($H_{II}$), and sponge ($L_3$) phases at ambient temperature in excess of aqueous medium without heat treatment. Mixing of the inverted-cubic-phase-forming MO and the sponge-phase-forming GO components, in equivalent proportions (50/50 w/w), yields an inverted hexagonal ($H_{II}$) phase nanostructured carrier. Scattering models are applied for fitting of the experimental SAXS patterns and identification of the structural changes in the aqueous and lipid bilayer subcompartments. The possibility of transforming, at ambient temperature (20 °C), the bicontinuous cubic nanostructures into inverted hexagonal ($H_{II}$) or sponge ($L_3$) mesophases may facilitate novel biomedical applications of the investigated liquid crystalline self-assemblies.

## Introduction

Phase transitions from bicontinuous inverted cubic phases of hydrated monoglyceride lipids to inverted hexagonal ($H_{II}$) and other nonlamellar phases have often been induced by thermal or pressure stimuli.[1–4] For the pure glycerol monooleate/water system, the transition temperature from an inverted cubic to a $H_{II}$ phase is as high[1,2] as 95 °C. On the other hand, the transition from a diamond-type inverted cubic lipid phase to a bicontinuous fluid sponge ($L_3$) phase can be induced by incorporation of additives causing nonuniform swelling of the aqueous compartments in the self-assembled structure, decrease in interfacial curvature and disordering of the periodic cubic organization.[5–12]

The interest to investigate phase transitions, induced by changes in the composition of amphiphilic mixtures, is motivated by the enhanced capacity of liquid crystalline (LC) nonlamellar phases, based on lipid/water mixtures, to encapsulate either hydrophobic or hydrophilic compounds for pharmaceutical, nutraceutical, biotechnological or biomedical applications (drugs, proteins, peptides, vitamins, DNA, diagnostic imaging agents).[13–22] The notable efficiency of inverted cubic lipid structures for loading of guest biomolecules is related to the high interfacial area of their multicompartment architectures. Above a certain concentration of the additives, the double diamond-type (*Pn*3*m* space group) inverted cubic phase can transform into self-assembled structures with lower or higher curvatures.[4–6,11,15–22] A dependence of the drug loading and release on the type of the liquid-crystalline phase has been established.[23–26] It is apparent that structural studies of multi-component mixtures of amphiphiles could facilitate finding compositions for which the phase transitions of the desired LC states occur at ambient or body temperatures relevant to drug processing or delivery.

Small-angle X-ray (SAXS) and neutron (SANS) scattering investigations are central methods for relatively high-resolution investigation of liquid crystalline structures.[27–53] The interpretation of the SAXS data is sometimes complicated owing to the purity state of the investigated commercial lipid products. Industrial grade products, such as phytantriol and glycerol monooleate, exhibit differences in their phase transition temperatures depending on the commercial source. Small amounts of impurities may not be indicated by the suppliers. Dong *et al.*[19] have shown that phytantriol from Roche and from BASF are characterized by differences in the shapes of the SAXS curves as well as in the temperatures of phase transition from an inverted cubic to an inverted hexagonal ($H_{II}$) phase.

[a] *Department of Chemistry and iNANO Interdisciplinary Nanoscience Centre, Aarhus University, 8000 Århus, Denmark*
[b] *Institute of Macromolecular Chemistry, Academy of Sciences of the Czech Republic, Heyrovskeho Nam. 2, 16206 Prague, Czech Republic*
[c] *CNRS UMR8612 Physico-chimie-Pharmacotechnie-Biopharmacie, Univ Paris Sud, Châtenay-Malabry, F-92296 France. E-mail: Angelina.Angelova@u-psud.fr*
[d] *Institute of Biophysics, Bulgarian Academy of Sciences, BG-1113 Sofia, Bulgaria*
[e] *HASYLAB at DESY, Notkestr. 85, D-22603, Hamburg, Germany*
[f] *Institute of Materials Research, GKSS Research Center, Geesthacht, D-21502, Germany*

† This article was submitted as part of a special collection on scattering methods applied to soft matter, marking the 65th birthday of Professor Otto Glatter.

View Article Online

Published on 16 November 2010. Downloaded by Lund University on 03/12/2014 13:54:28.

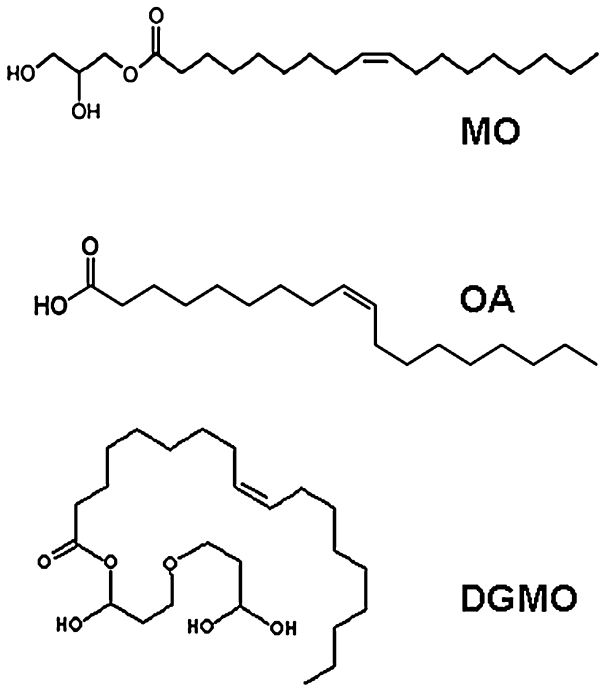


**Fig. 1** Chemical structures of glycerol monooleate/glycerol monooleate (MO), oleic acid (OA), and diglycerol monooleate (DGMO). MO constitutes the lipid product from Sigma-Aldrich, while GO from NOF Co. is a mixture of MO (main component), OA and GDMO (small amounts).

In this work we compare the SAXS patterns of liquid crystalline phases formed by self-assembly of two commercial glycerol monooleate products at full hydration. Both materials should form bicontinuous inverted cubic phases upon hydration at room temperature. However, they displayed different capacities to hydrate in excess aqueous phase. SAXS investigations were performed, at a constant ambient temperature, of the compositional dependence of the 'melting' of the bicontinuous inverted cubic self-assembled LC phase of glycerol monooleate (MO from Sigma-Aldrich) upon addition of increasing amounts of pharmaceutical-grade isotropic phase glycerol monooleate (GO from NOF Corp., see Experimental) (Fig. 1).

## Results

In a binary mixture MO/GO, the commercial GO product could alter the cubic phase state of the hydrated monoglyceride lipid MO if the fractions of oleic acid (OA) and diglycerol monooleate (DGMO), present in GO as impurities, are of non-negligible amounts since they modify the interfacial curvature of the mixed lipid membrane. The effects of adding DGMO and oils such oleic acid on the hydration level of the monoglyceride assembly are anticipated to be opposite[30,31,39] as DGMO has a counter effect on the spontaneous curvature as compared to OA. It may increase the amount of solubilized water in the self-assembled structure.

Taking into account that GO is in a fluid isotropic state at ambient temperature, the weight ratios between the two types of commercial glycerol monooleates, MO (Sigma-Aldrich) and GO (NOF), were varied in the samples so as to cause order-to-disorder ('melting') phase transitions of the bicontinuous double-diamond inverted cubic phase of MO. Small-angle X-ray scattering patterns of MO/GO/buffer mixtures, with varying MO/GO ratios and increasing MO fraction, are presented in Fig. 2–4.

### 1. Scattering of pharmaceutical grade glycerol monooleate (GO) self-assembled in excess buffer phase

The GO/buffer sample exists as a stable phase-separated lyotropic lipid system in excess aqueous phase at ambient temperature. Upon visual inspection, it appears as a white self-assembled aggregate separated from the excess buffer phase.

Fig. 2a shows that the SAXS pattern of the GO material, self-assembled in excess phosphate buffer, displays a single broad correlation peak centred at $q = 0.178$ Å$^{-1}$ (Table 1). Such a peak is typical for fluid isotropic (FI) phases. The

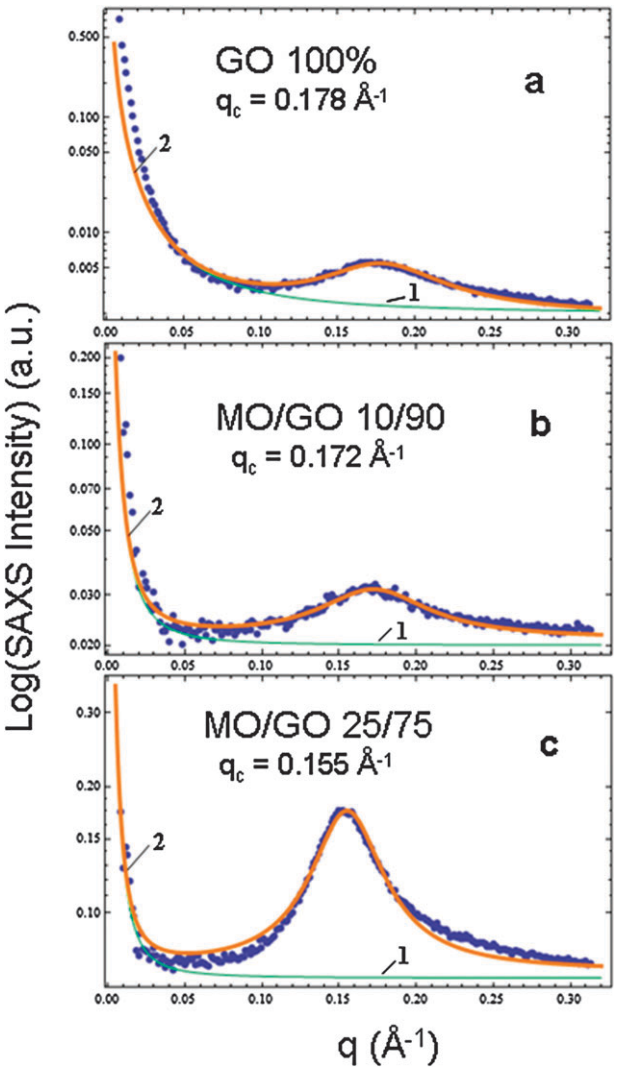


**Fig. 2** SAXS data (dots) with model fits of weakly hydrated sponge phases formed by pharmaceutical grade glycerol monooleate GO (a) and by MO/GO mixtures with weight ratios 10/90 (b) and 25/75 (c). The continuous lines (1) show scattering of the background. The continuous lines (2) show the sum of the sponge scattering and the background scattering. The temperature was 20 °C.

 This journal is © the Owner Societies 2011

View Article Online

Published on 16 November 2010. Downloaded by Lund University on 03/12/2014 13:54:28.

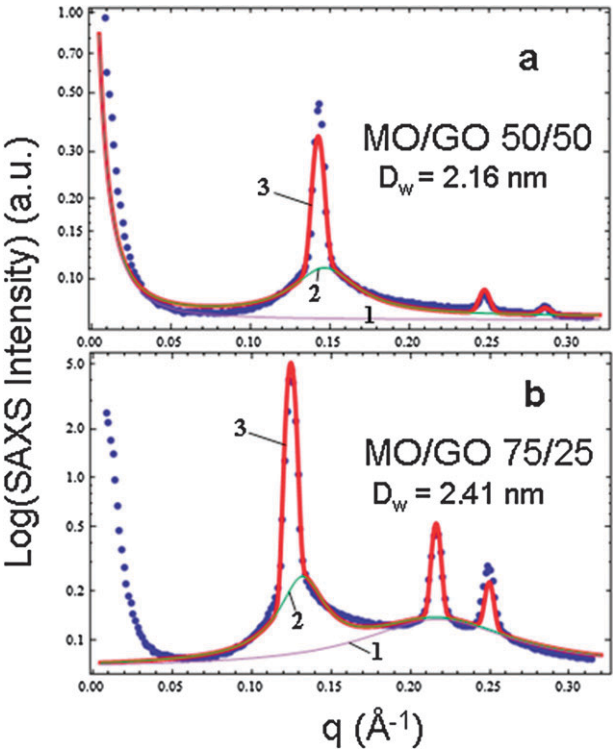


**Fig. 3** SAXS data (dots) with model fits of inverted hexagonal phases ($H_{II}$) coexisting with sponges in MO/GO mixtures with weight ratios 50/50 (a) and 75/25 (b). The temperature is 20 °C. The continuous lines (2) represent the scatterings resulting from the sponge cell–cell correlations. The line (1) corresponds to scatterings from background (a) or to bilayer correlations in weakly hydrated sponges (b). The curves (3) show the sum of the fitted $H_{II}$-phase scattering and the scattering of either the background (a) or the sponges (b).

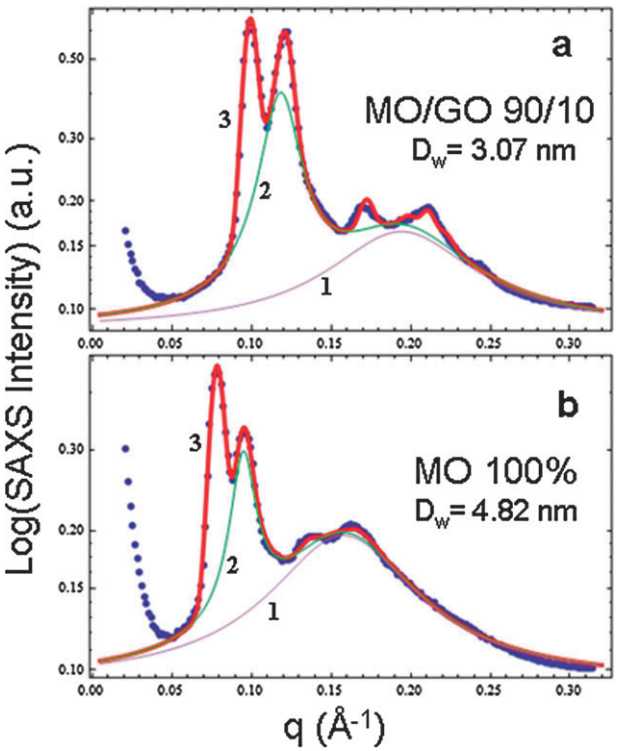


**Fig. 4** SAXS data (dots) with model fits of bicontinuous *Pn3m* inverted cubic phases coexisting with sponges in lipid mixtures with MO/GO weight ratios 90/10 (a) and 100/0 (b). The systems are hydrated in excess aqueous phase. The temperature is 20 °C. The continuous lines (3) show the sum of the scattering of the inverted cubic phase and the scattering of sponges that fits the experimental data. The curves (1) are scattering resulting from bilayer correlations in the sponge phase. The lines (2) show the sponge cell–cell correlations.

obtained pattern was excellently fitted by scattering (eqn (1)) from sponge ($L_3$) bilayer correlations (curve 2) superimposed on a decaying background (curve 1). The sponge ($L_3$) phase is a bicontinuous lipid bilayer phase, which does not display long-range crystalline order (see Fig. 5c below). This fluid phase may be considered as a 'molten cubic phase'. The fit of the SAXS peak, corresponding to the correlations between the lipid bilayers in the sponge, yields a characteristic distance of 3.53 nm. It is close to the bilayer thickness, $L$, of MO, which is around[54] 3.2 nm, but is essentially smaller than the lattice parameters of inverted cubic phases formed by lipids in excess water medium. The position of the correlation peak maximum ($q$ = 0.178 Å$^{-1}$), corresponding to a relatively short correlation distance, suggests that the hydration level of GO in this bicontinuous phase is low even under the excess water conditions. For comparison, the peaks maxima for the pure MO/water assemblies (see Fig. 4) yield a larger correlation distance and larger cell dimensions, which favour the entrapment of more water in the interior of the self-assembled LC structure.

The phase diagram of the pure MO/water system shows[2] that a fluid isotropic phase is not present under excess water conditions at ambient temperatures. In fact, a FI phase has been observed[2] with MO under limited hydration or upon heating of the $H_{II}$ phase of the hydrated lipid to temperatures above 100 °C. Therefore, a fluid isotropic phase, which lacks a periodic order, occurs in excess water upon dehydration of the $H_{II}$ phase.

## 2. Dependence of the scattering behaviour of the MO/GO mixtures on the sample composition

**2.1 Sponge swelling.** Upon addition of 10 wt% of MO to the pharmaceutical grade GO, the sponge correlation peak shifts to lower $q$ values (Table 1), representing an increase in the characteristic distance in the self-assembled MO/GO/buffer system (Fig. 2b). With further increase of the MO fraction to a weight ratio MO/GO of 25/75 (Fig. 2c), the bilayers correlation distance in the sponge rises to 4.05 nm. This value is bigger than the thickness of the MO bilayer. It should be noticed that the height of the peak observed at a MO/GO ratio of 25/75 (w/w) is higher than that of the broad SAXS peak arising from the bilayer correlations in the sponge phase of GO (Fig. 2a). The better defined SAXS peak and the higher intensity reflects increased structuring of the LC system. The nucleation and beginning of the 'crystallisation' of an inverted hexagonal lattice structure is supposed close to this composition. Considering the shift of the scattering maximum to lower $q$ values, the $H_{II}$ phase in the MO/GO mixture is anticipated to be more hydrated than the fluid sponge phase formed by GO alone.

View Article Online

Published on 16 November 2010. Downloaded by Lund University on 03/12/2014 13:54:28.

**Table 1** Parameters determined from fitting of the experimental SAXS patterns of the self-assembled lipid/buffer mixtures. The peak standard deviation was assumed equal for all peaks in the fit

| Lipid system (w/w) | Lattice parameter ($a$) or cell–cell distance/Å | Diameter of water channels $D_w$/Å | Thickness $L$/Å | Peak standard deviation $\sigma$/Å$^{-1}$ | 1st Peak position $q$/Å$^{-1}$ | 1st Corr. peak of sponge $q_{c1}$/Å$^{-1}$ | 2nd Corr. peak of sponge $q_{c2}$/Å$^{-1}$ | 1st Corr. length $\xi_1$/Å | 2nd Corr. length $\xi_2$/Å |
|---|---|---|---|---|---|---|---|---|---|
| MO 100% | Inverted cubic *Pn3m* 112.7 | 48.2 | 31.5 | 0.004 | 0.078 | 0.095 | 0.157 | 116 | 21 |
| MO/GO 90/10 | Inverted cubic *Pn3m* 89.2 | 30.7 | 32.4 | 0.004 | 0.099 | 0.118 | 0.194 | 78 | 20 |
| MO/GO 75/25 | Inverted hex ($H_{II}$) 58.0 | 24.1 | 33.9 | 0.003 | 0.125 | 0.132 | 0.217 | 73 | 20 |
| MO/GO 50/50 | Inverted hex ($H_{II}$) 50.7 | 21.6 | 29.1 | 0.003 | 0.143 | 0.147 | | 44 | |
| MO/GO 25/75 | Fluid $L_3$ 40.5 | | | | | 0.155 | | 42 | |
| MO/GO 10/90 | Fluid $L_3$ 36.5 | | | | | | 0.172 | | 25 |
| GO 100% | Fluid $L_3$ 35.3 | | | | | | 0.178 | | 25 |

**2.2 Inverted hexagonal lattice growth.** The SAXS patterns shown in Fig. 3 are identified as coming from inverted hexagonal ($H_{II}$) phases in the MO/GO mixtures. The data were fitted using (3). At equal quantities of the components MO/GO of 50/50 (w/w), the inverted hexagonal phase (Fig. 3a) has a lattice parameter $a_h$ = 5.07 nm (Table 1). The $H_{II}$ phase is accompanied by a small amount of a sponge phase that has a peak positioned very close to the first peak of the inverted hexagonal phase (Table 1). The augmentation of the MO quantity in the MO/GO mixture (Fig. 3b) causes a growth of the intensities of the inverted hexagonal phase peaks from the broad sponge correlation peak. The bilayers correlation distance in the sponge increases to 4.27 nm at a MO/GO ratio of 75/25 (w/w). The $H_{II}$ lattice parameter rises to $a_h$ = 5.8 nm as well (Fig. 3b).

The fitting of the experimental SAXS data (Fig. 3b) yielded two distinct maxima in the background described as sponge-type correlations: sponge cell–cell correlations and correlations between the lipid bilayers. The sponge cell correlation length is $L$ = 4.76 nm for the first maximum, while the second one is characterized by a distance $L$ = 2.9 nm. For comparison, the thickness of two adjacent lipid monolayers in the $H_{II}$ structure was found to be 3.39 nm in the performed fitting. It could be speculated that the dry lipid regions in the $H_{II}$ phase are centred on the junctions between three lipid monolayers (Fig. 5b). The utilized fitting model may be further developed in order to properly include the internal hydrophobic regions in the $H_{II}$ phase.

The increase in the lattice parameter with increasing MO content indicates an increase in the amount of solubilized water content. This explains the transition to inverted cubic phase at a high MO content in the self-assembled system.

**2.3 Bicontinuous *Pn3m* inverted cubic lattice growth.** Fig. 4 shows the SAXS data of samples in which the MO component is the dominant one, namely, its fraction in the MO/GO system is 90 wt% (a) or 100 wt% (b). The peak positions (Table 1) indicate that the obtained self-assembled lipid/buffer systems are evidently more hydrated and transform into double-diamond inverted cubic lattice (*Pn3m*) structures. The fit of the scattering curves is performed on the basis of eqn (2). The model assumes a constant thickness of the lipid bilayer and sharp lipid/water interfaces. The lipid bilayer thickness, $L$, was determined to be around 3.2 nm (Table 1), which is in agreement with previous determinations.[2,43,54] For MO alone, the cubic lattice exhibits $a$ = 11.27 nm, which is larger than in our previous measurement.[22] The increased lattice parameter could be attributed to the prolonged hydration period or to the effect of ionized species in the buffered system.

The analysis of the background revealed again the presence of two correlation peak maxima. The first one is characterized by a sponge cell–cell correlation distance 5.32 nm for the sample with 90 wt% MO in the MO/GO mixture (Fig. 4a) whereas it is 6.6 nm for the MO/buffer sample (Fig. 4b). The second maximum yields bilayer correlation distances of 3.23 nm and 4.00 nm, respectively, in the two samples. It appears that the bilayers correlation distance of the sponge cells in the MO/GO 90/10 (w/w) system and the thickness, $L$, of the lipid bilayer in the bicontinuous inverted cubic phase are equal. Hence, the cubic membrane geometry seems to favour equivalent bilayer distances in the coexisting sponge fluid. Conversely, in the $H_{II}$ phase (Fig. 3), the hydrophobic monolayer regions appear to be compressed owing to the $H_{II}$ geometry.

## Discussion

The cubic 'melting' phase transitions are of both fundamental theoretical and practical interest.[6,38,55–61] One mechanism of 'melting' considers the lipid membrane fluctuations that are temperature sensitive. From a theoretical view point, the phase transition from an ordered cubic to a sponge membrane can be considered *via* a curvature model in which the energy of a given topology depends on both the mean curvature and the Gaussian curvature of the membrane.[56] The parameters in this model are the bilayer bending rigidity and the Gaussian curvature modulus. The periodic structure of the cubic phase may be perturbed by thermal fluctuations or excitations of the lipid bilayer. Such fluctuations will introduce defects that cause the 'melting' of the cubic liquid crystal to a sponge. The system remains bicontinuous, however the lipid bilayer forms a minimal surface that is not periodic.[55]

The present work uses a model for the scattering intensity of a sponge phase in which the correlation length $\xi$ is related to the fluctuations of the lipid bilayers. However, the thickness of the membrane could not be directly compared with the obtained correlation length because we did not use an absolute scale in the fitting procedure. Nevertheless, the model allows for absolute determination of the correlation length and estimation of when the lipid membrane will undergo strong shape fluctuations. Such fluctuations can break up the bicontinuous phase into membrane fragments[45]

 This journal is © the Owner Societies 2011

View Article Online

Published on 16 November 2010. Downloaded by Lund University on 03/12/2014 13:54:28.

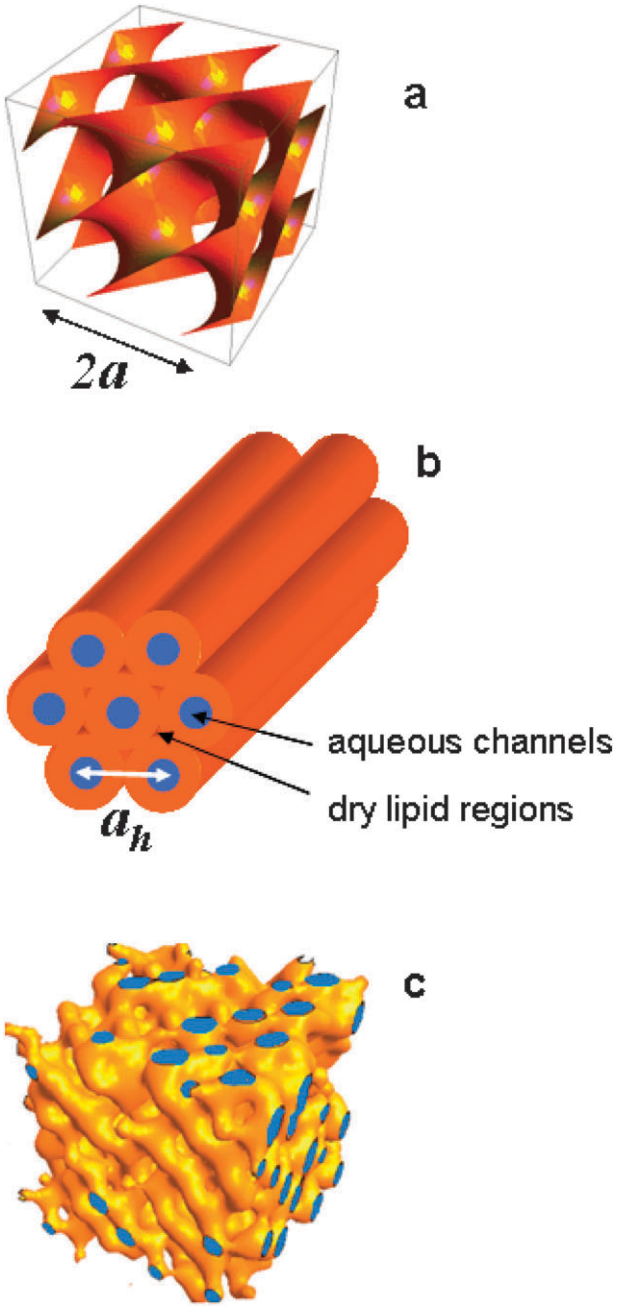


**Fig. 5** Schematic drawings of the structural elements constituting a bicontinuous inverted cubic liquid crystalline phase of the diamond (*Pn*3*m*) space group symmetry (a), an inverted hexagonal ($H_{II}$) phase (b), and a fluid sponge ($L_3$) phase (c). The lattice parameter is denoted by *a*.

or micellar aggregates[15,16,62,63] and the lipid membrane will undergo a topological change.

The $L_2$ phase formation was investigated by de Campo *et al.*[31] The authors have suggested[31] for a similar monoglyceride (the monolinolein (MLO)/water system) that this isotropic phase most likely has a locally flat structure (probably consisting of bilayers), similar to the $L_3$ structure. When the sample is fully hydrated, this phase exists in excess water (Winsor II micellar solution). In the present study, the formation of sponge-like structure in excess water (in the biphasic region) is suggested. The possible ways for fragmentation of the liquid crystalline phase formed by GO in excess buffer is outside the scope of the present study. The solubilization of the $L_3$ phase by a detergent should be additionally investigated in order to find out the conditions for an eventual sponge-to-reverse micelle phase transition.

The second mechanism of 'melting' refers to the changes in the lipid membrane composition at a constant temperature. The experimental phase sequence established in the present work as a function of the composition of the MO/GO amphiphilic system is:

$$\text{Inverted Cubic } (Pn3m) \rightarrow \text{Inverted Hexagonal } (H_{II}) \rightarrow \text{Sponge } (L_3) \text{ fluid phase.}$$

The observed phase transformation from an inverted cubic to a sponge phase ($L_3$) with increasing GO content (Fig. 2–4) occurs under full hydration conditions. Intermediate stages were found as a function of the mixed composition and they involve a tendency towards more negative interfacial curvature and formation of an inverted hexagonal phase (Fig. 3). The compositional 'melting' of the $H_{II}$ phase to a sponge $L_3$ phase at high GO fraction (Fig. 4) corresponds a loss of long-range order, but does not seem to involve a coexistence with a micellar phase. In fact, the observed topology of the compositional 'melting' of the inverted cubic *Pn*3*m* phase of MO is analogous to that of its temperature 'melting', which includes a structural transition to a $H_{II}$ phase as well. The phase sequence inverted cubic $\rightarrow$ $H_{II}$ $\rightarrow$ fluid isotropic (FI) phase, induced upon raising the temperature, has been well documented.[2] For the MO/water system, the transition from an inverted cubic to an inverted hexagonal phase occurs[1] at 95 °C. Further heating above 100 °C transforms the $H_{II}$ phase into isotropic fluid.

Here, the melting transition of the inverted cubic *Pn*3*m* phase is realized at room temperature. The compositional 'melting' effects could be explained by the *packing parameter* of the investigated amphiphiles defined as $\eta = V/(A_o \cdot l_H)$, where $V$ is the volume of the hydrocarbon chains, $l_H$ is the maximum effective hydrocarbon chain length, and $A_o$ is the optimal surface area per molecule defined at the polar/apolar interface. The packing parameter of the amphiphile glycerol monooleate MO, favouring nonlamellar structures, has been estimated[45] to be $\eta = 1.07$. Continuous changes in the monolayer curvature of the MO membrane can be induced by either pressure or temperature variation.[1–3] The inclusion of additives may promote the fine diminution of the interfacial curvature, leading to either cubic phase swelling or formation of lamellar phases, or to increase of the interfacial curvature and transformation to inverted hexagonal structures as more negatively curved assemblies.[5,6,31,42]

Diglycerol monooleate (DGMO), considered as an impurity in the investigated MO/GO mixtures, has been demonstrated[39] to be a lamellar-forming lipid owing to its extended polar headgroup. The lamellar phase ($L_\alpha$) of DGMO exists up to a water content of about 40 wt%. In excess aqueous phase, the DGMO/water system exhibits a coexistence of a lamellar $L_\alpha$ phase and a fluid isotropic micellar $L_1$ phase.[39] The MO/DGMO/water (30/20/50 or 44/16/40) self-assembled systems

View Article Online

Published on 16 November 2010. Downloaded by Lund University on 03/12/2014 13:54:28.

are characterized[39] by an inverted cubic *Ia*3*d* phase, which transforms into an inverted cubic *Pn*3*m* phase at lower DGMO percentages (*i.e.* 53/7/40). For MO/DGMO/water mixtures with elevated DGMO content above 25 wt%, the ($L_\alpha$) phase has been a dominant one even at low hydration levels.[39] Considering the preference of DGMO for structural transformations towards less curved (lamellar $L_\alpha$ phase) fluid structures, this lipid was suggested to stabilize, at high proportions of GO in the samples investigated here, the lower-curvature phase, namely the sponge phase.

At high MO fractions in the mixtures, such as 75 wt% (Fig. 3), the fitting of the scattering intensity yielded two characteristic correlation lengths in the background scattering. One of them represents the bilayers correlations and the second one is related to the sponge cell–cell correlations. The sponge effects are apparently pronounced in the presence of additives in the samples.

While DGMO appears to promote fluid bilayer phases under excess water conditions, the oleic acid (OA) additive has been found[30] to favour the $H_{II}$ phase formation upon mixing with MO. The hydrated MO/OA mixtures have revealed complex phase diagrams.[16,18,26,27,30,62–65] Oleic acid may self-assemble alone into an *Fd*3*m* micellar cubic phase.[30] It does not form lamellar bilayer phases alone without the addition of a co-lipid. It has been shown[30] that mixing of the cubic phase-forming lipid MO with OA, which has a propensity to assemble into an *Fd*3*m* micellar cubic phase, results in the formation of an inverted $H_{II}$ liquid crystalline phase.

OA was suggested to impart a more hydrophobic character to the MO/water assembly since its inclusion into the MO membrane considerably reduces the hydration of the self-assembled system, which transforms into an $H_{II}$ phase. Nakano *et al.*[30] have reported a dependence of the lattice parameter of the $H_{II}$ phase on the weight ratio between the MO and OA components in the mixture. They have determined the following lattice parameters: $a_h$ = 6.42 nm at MO/OA 5/5 (w/w), $a_h$ = 6.20 nm at MO/OA 4/6 (w/w), and $a_h$ = 5.80 nm at MO/OA 3/7. Our result $a_h$ = 5.80 nm obtained at MO/GO 75/25 (w/w) (Fig. 3b) coincides with the $a_h$ value for the MO/OA 3/7 mixture,[30] in which a DGMO component is not present. These data confirm that the inclusion of OA additive changes the curvature of the MO membrane to more negative magnitudes and stabilizes the $H_{II}$ phase.

In the pharmaceutical-grade monoglyceride (GO), the OA and DGMO constituents were detected as impurities with regard to the lipid MO in the mixed assemblies. In fact these compounds have often been added to MO in several works in order to functionalize the LC structures[16,18,26,27,30,39,62–65] or cubosome particles.[30,40] Therefore, the OA and DGMO impurities are not harmful for the investigated pharmaceutical multicompartment systems.

Quite often a sponge phase has been observed upon swelling of the MO/water inverted cubic phase.[5–12,38] The SAXS maximum of this highly hydrated phase has been determined at $q$ around 0.05–0.06 $Å^{-1}$. According to Qiu and Caffrey,[2] the formation of a fluid isotropic phase of MO is favoured at low hydration levels or upon dehydration of the $H_{II}$ phase at temperatures above 100 °C. Borné *et al.*[62] have suggested that the isotropic phase, induced in MO/OA assemblies at high temperatures, is a reverse micellar $L_2$ phase. A fluid isotropic phase of MO, which is suggested to have a fragmented bilayer membrane topology at high temperatures, has not yet been analysed at ambient temperatures under excess water conditions as in this work.

Recent cryo-TEM investigations[60,61] have demonstrated that the melting $H_{II}$-to-$L_3$ structural phase transition can occur in monoglyceride-based LC aqueous dispersions by adjusting the percentages of the amphiphilic components. Nanoparticles with an $H_{II}$ phase internal structure have been obtained in a mixed system DGMO/GDO/F127/$H_2O$ (2.25/2.25/0.5/95.0), where GDO is dioleoyl glycerol and F127 is a Pluronic type co-surfactant. Sponge-type internal structures have been established in DGMO/GDO/P80/$H_2O$ (2.13/2.13/0.74/95.0) nanodispersions (P80 denotes the non-ionic surfactant Polysorbate 80 (Tween 80)). While the employed DGMO/DGO ratio has been demonstrated to favour the $H_{II}$ phase structure,[60,61] the transition from an $H_{II}$ phase to a sponge organization has been considered to be due to the less negative curvature introduced by the non-ionic surfactant Polysorbate 80. In such systems, a phase separation between an $L_3$ phase and other coexisting phases has been established at the submicron scale.[61]

## Conclusion

The means of tuning the aqueous and membrane compartments as well as the supramolecular organization of amphiphilic nanocarriers are crucial for preparation of membrane-type lipid particles with internal structures (spongosomes, hexosomes, cubosomes). In the present work we analyzed the SAXS data of amphiphilic mixtures approaching in complexity the sophisticated pharmaceutical formulations. In controlled drug release studies in excess water phase, it is sometimes desirable to decrease the inverted cubic-to-inverted hexagonal phase transition temperature down to physiological or ambient temperatures. This is anticipated to provide slow release profiles from the channels of the liquid crystalline $H_{II}$ phase nanocarrier.

In the present work, the phase transition sequence, inverted cubic → $H_{II}$ → sponge ($L_3$) phase, is realized at ambient temperature without the application of high pressure or thermal heating stimuli. The investigated monoglyceride products MO and GO displayed different capacities to hydrate. MO forms a bicontinuous inverted cubic phase in phosphate buffer and it mixes with the components MO, OA, and DGMO present in the GO product. Among them, OA causes considerable dehydration of the mixed assemblies. The addition of OA simultaneously affects also the packing of the fatty acyl chains as described in ternary monoglycerides/oil/water systems. The obtained SAXS results with the MO/GO mixtures revealed an order-to-disorder melting transition of a liquid crystalline phase in which the bilayer correlations are preserved. Sponge scattering is present in all samples, which confirms that the multicomponent composition, such as that in multicompartment nanovector preparations for pharmaceutical applications, will favour the structural disordering of the MO ideal cubic phase.

 This journal is © the Owner Societies 2011

View Article Online

Published on 16 November 2010. Downloaded by Lund University on 03/12/2014 13:54:28.

## Experimental

### 1 Materials and sample preparation

Powder of 1-monooleoyl-*rac*-glycerol (MO) [C18:1c9, $M_W$ 356.54 g mol$^{-1}$, purity 99%] was purchased from Sigma-Aldrich (France). Pharmaceutical-grade monoglyceride [C18:1, *cis*-9 glycerol monooleate, Japanese Pharmaceutical Excipient, >99% oleic acid ultra-purity, NOFABLE GO-991] for drug delivery applications was received from the NOF Corporation (Japan). The NOF's glycerol monooleate (denoted here as GO) is an isotropic liquid product at room temperature, different in appearance from the white powder of MO received from Sigma Co. Because of this difference in the physical state, the lipid product GO was analyzed by electrospray mass spectrometry (ESI-MS, Esquire-LC, Bruker) in positive and negative ion modes. The obtained ESI-MS and NMR spectra revealed that GO appears to be a mixture of glycerol monooleate (MO) ($M_W$ 356.54 g mol$^{-1}$), oleic acid (OA) ($M_W$ 282.46 g mol$^{-1}$) and diglycerol monooleate (DGMO) ($M_W$ 430.62 g mol$^{-1}$). The three compounds (Fig. 1) have the same hydrophobic (C18:1) chain but different polar headgroups. However, the supplier did not provide the exact proportions of the satellite compounds (OA and DGMO) in the pharmaceutical grade glycerol monooleate preparation (NOFABLE GO-991). Phosphate buffer ($NaH_2PO_4/Na_2HPO_4$, 1 : 1 mol/mol, $1 \times 10^{-2}$ M, pH 7, p.a. grade, Fluka) was prepared using MilliQ water (Millipore).

The samples for the SAXS investigations of the composition dependence of the melting of the self-assembled inverted cubic phase of MO upon addition of increasing amounts of fluid phase monoglyceride GO were prepared by weighing appropriate amounts of the two products and hydration of the melted mixtures in excess phosphate buffer phase (30 wt% amphiphile, 70 wt% buffer solution). The MO/GO weight ratio was varied in a broad range: 100/0, 90/10, 75/25, 50/50, 25/75, 10/90, and 0/100 (w/w). For every sample, eight cycles of vortexing (for 1 min) and incubation (for 5 min) were applied. The samples were left to equilibrate at 4 °C for long times before SAXS measurements.

### 2 Small-angle X-ray scattering (SAXS) measurements

The SAXS experiments were performed at ambient temperature (20 °C) using the modified NanoSTAR instrument[51] at the Department of Chemistry, Aarhus University. The instrument is the prototype of the commercially available SAXS equipment from Bruker-AXS. It has been optimized with respect to flux and background and therefore is ideally suited for solution scattering measurements.

The samples were filled in glass capillaries with a diameter of 1.7 mm. The distance between the sample and the HiSTAR position-sensitive gas detector was 64.7 cm. This distance allowed measurements in the $q$-range interval from 0.008 to 0.32 Å$^{-1}$. The beam diameter at the sample position was 1 mm. The X-ray exposure time was 15 min for samples forming inverted cubic and inverted hexagonal phase structures, 20 min for the MO/GO 25/75 (w/w) sample, 30 min for the MO/GO 10/90 (w/w) mixture, and 60 min for GO (100/0) hydrated in buffer. The background subtraction and all necessary normalizations were performed using the SUPERSAXS package (C.L.P. Oliveira and J.S. Pedersen, unpublished). The final intensity, $I$, is displayed as a function of the modulus of the scattering vector $q = (4\pi/\lambda)\sin(\theta)$, where $\lambda$ = 1.54 Å is the X-ray wavelength and $2\theta$ is the angle between the incident and scattered X-rays.

Preliminary small-angle scattering measurements (not shown in this paper) were done also at the B1 beamline (DORIS III synchrotron radiation ring, Hasylab/DESY, Hamburg) and at SANS1 beamline (FRG1 Neutron reactor, GKSS, Geesthacht).

### 3 SAXS data fitting and analysis

The experimental SAXS data were fitted with the following models of the scattering intensity.

**3.1 Scattering from a sponge.** The structure factor describing the broad peak centered at $q_c$ represents the cell–cell bilayer correlations[52] with a correlation length, $\xi$:

$$I(q) = \frac{c}{\xi^{-2} + (q - q_c)^2}, \tag{1}$$

The sponge cell has a characteristic dimension $L = 2\pi/q_c$ resulting from the lipid bilayer correlations. The intensity normalization constant is denoted by $c$.

**3.2 Scattering from a bicontinuous inverted cubic phase.** The model of Clerc, Dubous-Violette, Garstecki and Hołyst[50,53] was used to determine the structural parameters of the diamond inverted cubic lattice structure and the average water channel diameter, $D_w$. In this model, the lipid bilayer thickness, $L$, in the cubic lipid phase is assumed to be a constant throughout. The intensity of the cubic phase and the background, modelled as the scattering of two sponges, is:

$$I(q) = \frac{c_1}{q^2}\sum_{hkl}\exp\left[-\frac{(q - q_{hkl})^2}{2\sigma^2}\right]I_{hkl} + \frac{c_2}{\xi_1^{-2} + (q - q_{c1})^2} + \frac{c_3}{\xi_2^{-2} + (q - q_{c2})^2}, \tag{2}$$

where the first term describes the inverted cubic phase scattering and the second and third terms correspond to the bilayer cell–cell correlations (see (1)). The peak positions are denoted by $q_{hkl}$ and $q_{c1}$ and $q_{c2}$, respectively. The peak widths for all peaks of the inverted cubic phase are considered to be the same and described by $\sigma$. The correlation length is $\xi_1$ and $\xi_2$, respectively, while the constants $c_1$, $c_2$, and $c_3$ describe the intensity normalization. The cubic phase individual peak maximal intensities are given by $I_{hkl}$. The model scattering intensities are defined as

$$I_{hkl}(L) = M_{hkl}\left[F_{hkl}^{S*}\frac{\sin[\alpha_{hkl}\pi(h^2 + k^2 + l^2)^{1/2}L^*]}{\alpha_{hkl}2\pi(h^2 + k^2 + l^2)^{1/2}}\right]^2, \tag{3}$$

where $L^* = L/a$ is the dimensionless lipid layer thickness, $a$ is the unit cell parameter, $F_{hkl}^{S*}$ is the dimensionless structure factor, $M_{hkl}$ is a multiplicity factor, and $\alpha_{hkl}$ are correction parameters for particular cubic lattices. Having done the fitting for $L$, the value of $D_w$ was determined from the relationship $D_w = 0.707a - L$. Our nonlinear least-squares fitting algorithm is based on the well known Levenberg–Marquardt method.

View Article Online

Published on 16 November 2010. Downloaded by Lund University on 03/12/2014 13:54:28.

**3.3 Scattering from a hexagonal phase.** The model for the scattering from a hexagonal phase, which is utilized here, is a simplified version of the model of Sundblom *et al.*[49] The intensity is given by

$$I(q) = (\rho_1 - \rho_2)^2 n_d \langle F(q)^2 \rangle [1 + \beta(q) G(q)(\langle Z(q) \rangle - 1)], \quad (4)$$

where $\rho_1$ and $\rho_2$ are the electron densities of the water and the lipid, $n_d$ is the number density of particles, $F(q)$ is the form factor that can be expressed as a product of the form factor $P_{rod}$ of an infinitely thin rod and the cross-section form factor $P_{CS}(q)$ for solid cylinders:

$$\langle F(q)^2 \rangle = P(q) = P_{rod}(q) P_{CS}(q)$$

$$P_{rod}(q) = 2\mathrm{Si}(qL_h)/(qL) - \left[\frac{\sin(qL_h/2)}{qL_h/2}\right]^2,$$

$$P_{CS}(q) = \left(\frac{2J_1(qR)}{qR}\right)^2. \quad (5)$$

Here $\mathrm{Si}(x) = \int_0^x t^{-1} \sin(t) \mathrm{d}t$, $L_h$ is the length of the cylinder, $J_1(x)$ is the first-order Bessel function of a first kind, and $R = D_w/2$, where $D_w$ is the diameter of the water cylinder. The polydispersity of cylinders enters the factor $\beta(q)$, however it was not taken into account, *i.e.* $\beta(q) = 1$.

The distortions of the hexagonal lattice by disorder was accounted for by addition of a disorder factor, which is similar to the Debye–Waller factor that describes thermal vibrations in crystals:

$$G(q) = \exp(-\sigma_a^2 a_h^2 q^2), \quad (6)$$

where $a_h$ is the hexagonal lattice parameter, $\sigma_a^2$ is the relative mean square displacement around the average position of the cylinder.

The hexagonal lattice structure factor is given by:

$$\langle Z(q) \rangle = Z_0(q) = \frac{c_4}{q} \sum_{hk} \exp\left[-\frac{(q - q_{hk})^2}{2\sigma^2}\right] m_{hk}, \quad (7)$$

where $m_{hk}$ is the multiplicity factor and $c_4$ is a scaling factor. The peak shape is assumed to be Gaussian with a standard deviation of $\sigma$.

## Acknowledgements

The NMI3 research project for SANS measurements at FRG1 research reaktor, Geestchacht has been supported by the European Commission under the 6th Framework Programme through the Key Action: Strengthening the European Research Area, Research Infrastructures. Contract no.: RII3-CT-2003-505925. The authors acknowledge the reviewers' comments.

## References

1 C. Czeslik, R. Winter, G. Rapp and K. Bartels, *Biophys. J.*, 1995, **68**, 1423–1429.
2 H. Qiu and M. Caffrey, *Biomaterials*, 2000, **21**, 223–234.
3 C. E. Conn, O. Ces, X. Mulet, S. Finet, R. Winter, J. M. Seddon and R. H. Templer, *Phys. Rev. Lett.*, 2006, **96**, 108102.
4 A. Angelova, M. Ollivon, A. Campitelli and C. Bourgaux, *Langmuir*, 2003, **19**, 6928–6935.
5 K. Alfons and S. Engstrom, *J. Pharm. Sci.*, 1998, **87**, 1527–1530.
6 V. Cherezov, J. Clogston, M. Z. Papiz and M. Caffrey, *J. Mol. Biol.*, 2006, **357**, 1605–1618.
7 A. B. Wöhri, L. C. Johansson, P. Wadsten-Hindrichsen, W. Y. Wahlgren, G. Fischer G, R. Horsefield, G. Katona, M. Nyblom, F. Oberg, G. Young, R. J. Cogdell, N. J. Fraser, S. Engström and R. Neutze, *Structure (London)*, 2008, **16**, 1003–1009.
8 S. Abe and H. Takahashi, *Chem. Phys. Lipids*, 2007, **147**, 59–68.
9 S. Engström, K. Alfons, M. Rasmusson and H. Ljusberg-Wahren, *Prog. Colloid Polym. Sci.*, 1998, **108**, 93–98.
10 A. Ridell, K. Ekelund, H. Evertsson and S. Engström, *Colloids Surf., A*, 2003, **228**, 17–23.
11 A. Imberg, H. Evertsson, P. Stilbs, M. Kriechbaum and S. Engström, *J. Phys. Chem. B*, 2003, **107**, 2311–2318.
12 H. Evertsson, P. Stilbs, G. Lindblom and S. Engström, *Colloids Surf., B*, 2002, **26**, 21–29.
13 D. McLoughlin, M. Imperor-Clerc and D. Langevin, *ChemPhysChem*, 2004, **5**, 1619–1623.
14 J. C. Shah, Y. Sadhale and D. M. Chilukuri, *Adv. Drug Delivery Rev.*, 2001, **47**, 229–250.
15 J. Borné, T. Nylander and A. Khan, *J. Phys. Chem. B*, 2002, **106**, 10492–10500.
16 J. Borné, T. Nylander and A. Khan, *Langmuir*, 2002, **18**, 8972–8981.
17 J. Clogston and M. Caffrey, *J. Controlled Release*, 2005, **107**, 97–111.
18 L. B. Lopes, D. A. Ferreira, D. de Paula, M. T. J. Garcia, J. A. Thomazini, M. C. A. Fantini and M. V. L. B. Bentley, *Pharm. Res.*, 2006, **23**, 1332–1342.
19 Y.-D. Dong, A. W. Dong, I. Larson, M. Rappolt, H. Amenitsch, T. Hanley and B. J. Boyd, *Langmuir*, 2008, **24**, 6998–7003.
20 T. Mishraki, D. Libster, A. Aserin and N. Garti, *Colloids Surf., B*, 2010, **75**, 47–56.
21 J. Kraineva, V. Smirnovas and R. Winter, *Langmuir*, 2007, **23**, 7118–7126.
22 A. Angelova, B. Angelov, B. Papahadjopoulos-Sternberg, M. Ollivon and C. Bourgaux, *J. Drug Delivery Sci. Technol.*, 2005, **15**, 108–112.
23 G. A. Kossena, W. N. Charman, B. J. Boyd and C. J. H. Porter, *J. Controlled Release*, 2004, **99**, 217–229.
24 S. B. Rizwan, T. Hanley, B. J. Boyd, T. Rades and S. Hook, *J. Pharm. Sci.*, 2009, **98**, 4191–4204.
25 K. W. Y. Lee, T. Nguyen, T. Hanley and B. J. Boyd, *Int. J. Pharm.*, 2009, **365**, 190–199.
26 W. K. Fong, T. Hanley and B. J. Boyd, *J. Controlled Release*, 2009, **135**, 218–226.
27 P. Mariani, V. Luzzati and H. Delacroix, *J. Mol. Biol.*, 1988, **204**, 165–188.
28 V. Luzzati, R. Vargas, A. Gulik, P. Mariani, J. M. Seddon and E. Rivas, *Biochemistry*, 1992, **31**, 279–285.
29 F. Caboi, G. S. Amico, P. Pitzalis, M. Monduzzi and K. Larsson, *Chem. Phys. Lipids*, 2001, **109**, 47–62.
30 M. Nakano, T. Teshigawara, A. Sugita, W. Leesajakul, A. Taniguchi, T. Kamo, H. Matsuoka and T. Handa, *Langmuir*, 2002, **18**, 9283–9288.
31 L. de Campo, A. Yaghmur, L. Sagalowicz, M. E. Leser, H. Watzke and O. Glatter, *Langmuir*, 2004, **20**, 5254–5261.
32 A. Salonen, S. Guillot and O. Glatter, *Langmuir*, 2007, **23**, 9151–9154.
33 A. Yaghmur and O. Glatter, *Adv. Colloid Interface Sci.*, 2009, **147–148**, 333–342.
34 G. C. Shearman, A. I. I. Tyler, N. J. Brooks, R. H. Templer, O. Ces, R. V. Law and J. M. Seddon, *J. Am. Chem. Soc.*, 2009, **131**, 1678–1679.
35 P. Vandoolaeghe, J. Barauskas, M. Johnsson, F. Tiberg and T. Nylander, *Langmuir*, 2009, **25**, 3999–4008.
36 Y.-D. Dong, A. J. Tilley, I. Larson, M. J. Lawrence, H. Amenitsch, M. Rappolt, T. Hanley and B. J. Boyd, *Langmuir*, 2010, **26**, 9000–9010.
37 K. Bryskhe, K. Schillén, U. Olsson, A. Yaghmur and O. Glatter, *Langmuir*, 2005, **21**, 8597–8600.
38 S. Engström, P. Wadsten-Hindrichsen and B. Hernius, *Langmuir*, 2007, **23**, 10020–10025.

 This journal is © the Owner Societies 2011

View Article Online

Published on 16 November 2010. Downloaded by Lund University on 03/12/2014 13:54:28.


39 P. Pitzalis, M. Monduzzi, N. Krog, H. Larsson, H. Ljusberg-Wahren and T. Nylander, *Langmuir*, 2000, **16**, 6358–6365.
40 M. Nakano, A. Sugita, H. Matsuoka and T. Handa, *Langmuir*, 2001, **17**, 3917–3922.
41 M. Uyama, M. Nakano, J. Yamashita and T. Handa, *Langmuir*, 2009, **25**, 4336–4338.
42 B. Angelov, A. Angelova, M. Ollivon, C. Bourgaux and A. Campitelli, *J. Am. Chem. Soc.*, 2003, **125**, 7188–7189.
43 B. Angelov, A. Angelova, V. M. Garamus, G. Le Bas, S. Lesieur, M. Ollivon, S. Funari, R. Willumeit and P. Couvreur, *J. Am. Chem. Soc.*, 2007, **129**, 13474–13479.
44 B. Angelov, A. Angelova, U. Vainio, V. M. Garamus, S. Lesieur, R. Willumeit and P. Couvreur, *Langmuir*, 2009, **25**, 3734–3742.
45 B. Angelov, M. Ollivon and A. Angelova, *Langmuir*, 1999, **15**, 8225–8234.
46 M. Gotter, T. Sottmann, M. Baciu, U. Olsson, H. Wennerstrom and R. Strey, *Eur. Phys. J. E*, 2007, **24**, 277–295.
47 R. Gomati, N. Bouguerra and A. Gharbi, *Physica B (Amsterdam)*, 2001, **299**, 101–107.
48 H. Bunjes and T. Unruh, *Adv. Drug Delivery Rev.*, 2007, **59**, 379–402.
49 A. Sundblom, C. L. P. Oliveira, A. E. C. Palmqvist and J. S. Pedersen, *J. Phys. Chem. C*, 2009, **113**, 7706–7713.
50 P. Garstecki and R. Holyst, *Langmuir*, 2002, **18**, 2529–2537; P. Garstecki and R. Hołyst, *Langmuir*, 2002, **18**, 2519–2528.
51 J. S. Pedersen, *J. Appl. Crystallogr.*, 2004, **37**, 369.
52 N. Lei, C. R. Safinya, D. Roux and K. S. Liang, *Phys. Rev. E: Stat. Phys., Plasmas, Fluids, Relat. Interdiscip. Top.*, 1997, **56**, 608.
53 M. Clerc and E. Dubois-Violette, *J. Phys. II*, 1994, **4**, 275.
54 S.-J. Marrink and D. P. Tieleman, *J. Am. Chem. Soc.*, 2001, **123**, 12383–12391.
55 E. I. Kats and M. I. Monastyrskii, *J. Exp. Theor. Phys.*, 2000, **91**, 1279–1285.
56 R. Lipowsky, *Nature*, 1991, **349**, 475–481.
57 N. González-Segredo and P. V. Coveney, *Phys. Rev. E: Stat., Nonlinear, Soft Matter Phys.*, 2004, **69**, 061501.
58 R. S. Saksena and P. V. Coveney, *J. Phys. Chem.*, 2008, **112**, 2950–2957.
59 T. Imura, H. Yanagishita, J. Ohira, H. Sakai, M. Abe and D. Kitamoto, *Colloids Surf., B*, 2005, **43**, 115–121.
60 J. Barauskas, M. Johnsson and F. Tiberg, *Nano Lett.*, 2005, **5**, 1615–1619.
61 J. Barauskas, A. Misiunas, T. Gunnarsson, F. Tiberg and M. Johnsson, *Langmuir*, 2006, **22**, 6328–6334.
62 J. Borné, T. Nylander and A. Khan, *Langmuir*, 2001, **17**, 7742–7751.
63 J. Borné, T. Nylander and A. Khan, *J. Colloid Interface Sci.*, 2003, **257**, 310–320.
64 Y. Aota-Nakano, S. J. Li and M. Yamazaki, *Biochim. Biophys. Acta, Biomembr.*, 1999, **1461**, 96–102.
65 D. A. Ferreira, M. V. L. B. Bentley, G. Karlsson and K. Edwards, *Int. J. Pharm.*, 2006, **310**, 203–212.